

Acute Slices of Mice Testis Seminiferous Tubules Unveil Spontaneous and Synchronous Ca^{2+} Oscillations in Germ Cell Clusters¹

Claudia Sánchez-Cárdenas,³ Adán Guerrero,³ Claudia Lydia Treviño,³ Arturo Hernández-Cruz,⁴ and Alberto Darszon^{2,3}

³Departamento de Genética del Desarrollo y Fisiología Molecular, Instituto de Biotecnología, Universidad Nacional Autónoma de México (UNAM), Cuernavaca, Morelos, México

⁴Departamento de Neurociencia Cognitiva, Instituto de Fisiología Celular, UNAM, Circuito exterior s/n, Ciudad Universitaria, México

ABSTRACT

Spermatogenic cell differentiation involves changes in the concentration of cytoplasmic Ca^{2+} ($[\text{Ca}^{2+}]_i$); however, very few studies exist on $[\text{Ca}^{2+}]_i$ dynamics in these cells. Other tissues display Ca^{2+} oscillations involving multicellular functional arrangements. These phenomena have been studied in acute slice preparations that preserve tissue architecture and intercellular communications. Here we report the implementation of intracellular Ca^{2+} imaging in a sliced seminiferous tubule (SST) preparation to visualize $[\text{Ca}^{2+}]_i$ changes of living germ cells in situ within the SST preparation. Ca^{2+} imaging revealed that a subpopulation of male germ cells display spontaneous $[\text{Ca}^{2+}]_i$ fluctuations resulting from Ca^{2+} entry possibly throughout Ca_v3 channels. These $[\text{Ca}^{2+}]_i$ fluctuation patterns are also present in single acutely dissociated germ cells, but they differ from those recorded from germ cells in the SST preparation. Often, spontaneous Ca^{2+} fluctuations of spermatogenic cells in the SST occur synchronously, so that clusters of cells can display Ca^{2+} oscillations for at least 10 min. Synchronous Ca^{2+} oscillations could be mediated by intercellular communication via gap junctions, although intercellular bridges could also be involved. We also observed an increase in $[\text{Ca}^{2+}]_i$ after testosterone application, suggesting the presence of functional Sertoli cells in the SST. In summary, we believe that the SST preparation is suitable to explore the physiology of spermatogenic cells in their natural environment, within the seminiferous tubules, in particular Ca^{2+} signaling phenomena, functional cell-cell communication, and multicellular functional arrangements.

calcium, cell coupling, intercellular communication, spermatogenesis, testis

INTRODUCTION

Spermatogenesis is a complex process that drives the differentiation of diploid spermatogonial cells into haploid mature spermatozoa in the testis. Spermatogenesis takes place

in the seminiferous tubules under strict physiological regulation that includes the interplay of paracrine hormones and intercellular communication among several cell types from the testis epithelium [1]. Inside the seminiferous tubules, Sertoli cells provide structural support and nourishment to spermatogenic cells through their secretory factors [2]. The correct interaction between Sertoli and spermatogenic cells is fundamental for the proper development of spermatogenesis. Disruption of these interactions can alter spermatogenesis and lead to infertility [3].

Ca^{2+} is a universal second messenger that regulates diverse physiological functions such as contraction, secretion, metabolism, proliferation, etc. [4]. Little is known about how Ca^{2+} regulates spermatogenesis and about the homeostatic mechanisms that control cytoplasmic Ca^{2+} concentration ($[\text{Ca}^{2+}]_i$) in cells from the seminiferous tubules. It is known that Sertoli cells display $[\text{Ca}^{2+}]_i$ increases in response to testosterone (T) [5] and follicle-stimulating hormone [6], two critical hormones that regulate spermatogenesis. This $[\text{Ca}^{2+}]_i$ increase mainly results from Ca^{2+} entry, which then regulates cell migration and proliferation [7]. Immunocytochemical and RT-PCR studies have shown that spermatogenic cells express ryanodine and inositol trisphosphate (InsP_3) receptors [8–10], as well as voltage-dependent Ca^{2+} channels, mainly Ca_v3 channels [11–14]. Ca_v3 channels are functionally expressed in spermatogenic cells, as shown by electrophysiological recordings [11, 15]. Furthermore, fluorometric experiments in rat round spermatids have shown $[\text{Ca}^{2+}]_i$ increases due to Ca^{2+} entry, as well as Ca^{2+} release from intracellular stores triggered by thapsigargin and ionomycin [16]. As in many cell types, $[\text{Ca}^{2+}]_i$ changes also regulate many of the main functions of mature sperm (reviewed in [13]).

Depending on the cell type and the physiological event, $[\text{Ca}^{2+}]_i$ increases can be transient, sustained, or oscillatory. Ca^{2+} oscillations are present in many endocrine tissues, such as pituitary [17], pancreas [18], and adrenal medullae [19], where they regulate basal hormone secretion [20]. In many cases, Ca^{2+} oscillations, whether spontaneous or stimulated, involve multicellular functional networks [21]. Recording of Ca^{2+} oscillations and other functional studies in such multicellular networks is only possible in intact organs or acute tissue slices. Unlike cultured or dispersed cells, these biological preparations preserve intercellular communications and the native repertoire of ionic channels, closely resembling the physiological environment of cells in situ.

The seminiferous epithelium has several types of intercellular junctions, such as tight and adherent junctions, which regulate the onset and maintenance of spermatogenesis [22, 23]. Gap junctions (GJs) allow another type of intercellular communication, in which plasma membrane channels directly interchange small molecules of <1 kDa (IP_3 , Ca^{2+} , and cAMP)

¹Supported by grants IN227910, IN225406, and IN202212-3 from DGAPA-UNAM; 79763, 9933, 102085, and 128566 from CONACyT (Consejo Nacional de Ciencia y Tecnología, México); and PICSA10-116 from ICYTDF (Instituto de Ciencia y Tecnología del Distrito Federal) to A.H.-C.; and National Institutes of Health grant R01 HD038082-07A1.

²Correspondence: E-mail: darszon@ibt.unam.mx

between connected cells [24, 25]. Connexins, structural proteins of GJs, are expressed in the seminiferous epithelium. Specifically, connexin 43 is abundantly expressed in rodent Sertoli and germ cells [26, 27]. The functionality of GJs in the seminiferous tubules has been assessed by diffusion of the fluorescent dye between pairs of Sertoli cells and between Sertoli and spermatogenic cells [26, 28]. Recently, it has been suggested that GJ couplings are involved in proliferation and apoptosis in mice testis [29]. Intercellular bridges (IBs), which result from the incomplete cytoplasm division of a group of germ cells, allow another type of cell-cell communication between syncytia of spermatogenic cells. Cells within a syncytium remain connected until they mature into fully differentiated spermatozoa [30]. The physiological role of the syncytium remains unexplained. Nonetheless, it is known that IBs participate in regulating the synchronous spermatid differentiation during spermatogenesis [31, 32].

Given the complex intercellular interactions in the seminiferous tubules, we implemented an acute slice preparation to characterize Ca^{2+} -signaling mechanisms in spermatogenic cells, in a biological context where intra- and intercellular communications are well preserved. Here we combine the sliced seminiferous tubule (SST) preparation with fluorescence Ca^{2+} imaging to visualize in real-time the Ca^{2+} fluctuations of germ cells inside the seminiferous tubules, in both basal and stimulated conditions.

Our results show for the first time remarkable oscillatory $[\text{Ca}^{2+}]_i$ changes in spermatogenic cells in a suitable preparation to explore their physiological behavior inside the acutely isolated seminiferous tubules.

MATERIALS AND METHODS

SST Preparation

Animal studies were performed under an institutional protocol similar to the USPHS: Guide for the Care and Use of Laboratory Animals and the Official Mexican Guide for the Care and Use of Laboratory Animals from the Secretary of Agriculture (SAGARPA NOM-062-Z00-1999). Adult Balb-c mice of 8 wk of age were used for these studies. Mice were maintained in the institute's animal facility and fed ad libitum. The animals were euthanized by decapitation under isoflurane anesthesia and testes were obtained by dissection under a stereomicroscope. The tunica albuginea of both testes was removed and the seminiferous tubules were mechanically untangled and dispersed with tweezers in a physiological solution that contained (mM) 125 NaCl, 2.5 KCl, 2 CaCl_2 , 1 MgCl_2 , 1.25 NaH_2PO_4 , 26 NaHCO_3 , 12 glucose; gassed with 5% CO_2 , 95% O_2 ; adjusted to pH 7.4; and embedded in 3% low-melting-point agarose (Invitrogen Catlab) dissolved in physiological solution at 25°C. The agarose containing the seminiferous tubules was hardened by immersion in ice-cold physiological solution, and the agar block was glued with cyanoacrylate onto the plate of a vibrating-blade microtome (Leica VT-1000S; Leica Microsystems CMS GmbH). Then, the slicing chamber was filled with physiological solution kept at 3°C and transverse slices of 160 μm in thickness were cut using a vibrating-blade microtome. As the seminiferous tubules are embedded in a random orientation, the tubules can be cut on sagittal, lateral, transversal, or diagonal orientations. Freshly cut SST were immediately transferred to an incubation beaker containing physiological solution at room temperature, and continuously gassed (5% CO_2 , 95% O_2) to maintain pH near 7.4. Slices remained viable for up to 5 h after preparation.

Spermatogenic Cell Dissociation Protocol

Freshly dissociated spermatogenic cells were obtained by sequential 10-min enzymatic digestions of the testis (without tunica, with collagenase [0.5 mg/ml] and trypsin [1 mg/ml]) in the same physiological medium as above. The cell suspension was washed once with 0.5% BSA and twice with medium without BSA. Fluo-4 AM loading and Ca^{2+} imaging were performed as in SST preparation.

Intracellular Ca^{2+} Imaging of Living Testis Slices

An SST was mounted on a plexiglass recording chamber and incubated for 30 min with physiological solution containing the cell-permeable fluorescent

Ca^{2+} indicator fluo-4AM (20 μM ; Invitrogen). Then, the slice was immobilized with a nylon mesh, placed on the stage of a microscope, and continuously perfused (2 ml/min) with gassed physiological solution. Experiments were performed at room temperature. The slice was viewed with an upright microscope (Nikon Eclipse 80i) and water-immersion fluorescence Nikon objectives (10 \times , 20 \times , and 40 \times). Fluo-4 was excited at 488 nm with monochromatic light (Polychrome V Illumination System; TILL Photonics), and emitted fluorescence was band passed with a Nikon a B2-E/C filter set. Fluorescent images were acquired with a cooled digital CCD camera (Imago QE; TILL Photonic) under protocols written in TILL vision software 4.0. Images were acquired every second with an exposure/illumination time of 10 ms for a total of 10 min (600 images).

Image Recording and Analysis

Image sequences (movies) were obtained under basal conditions during continuous perfusion with physiological saline. Movies were processed and analyzed with macros written in Image J (Version 1.38; National Institutes of Health). Raw movies were converted to $F = F(i) - F_0$, where F_0 is the fluorescence image formed by averaging the first 5 frames of the sequence and $F(i)$ represents each fluorescence image of the sequence. No attempts were made to calculate absolute $[\text{Ca}^{2+}]_i$ from these data. An $F(t)$ multicell plot from dozens of individual cells was generated with Igor Pro 5.03 macros (Wavemetrics, Inc.) written by León Islas, Ph.D. Facultad de Medicina UNAM. Here, ordinates represent cell number (one cell per row), the time is represented in the abscissa, and F values are color coded. Numerical data were plotted with Origin 6.0 (MicroCal Software) or Igor Pro.

Analysis of the Coupling of Spontaneous Ca^{2+} Oscillations

For each SST movie recorded, regions of interest were drawn by hand (one region per cell) and single-cell Ca^{2+} dynamics calculated over 600 sec. The data were exported to R software to perform principal component analysis (PCA) with the function *prcomp* [33].

PCA is a mathematical procedure that uses an orthogonal transformation to convert a set of observations of possibly correlated variables into a set of values of linearly uncorrelated variables called principal components [34]. PCA transforms the data to a new coordinate system such that the greatest variance by any projection of the data comes to lie on the first principal component (PC1), the second greatest variance on the second principal component (PC2), and so on. The analysis of at least three SST preparations revealed that $\approx 80\%$ of data variability is accounted by the first three principal components, PC1, PC2, and PC3 (Supplemental Fig. S1; all Supplemental Data are available online at www.biolreprod.org). To identify groups of correlation (cells showing coupled Ca^{2+} dynamics) we calculated a correlation coefficient (D_{corr} , a "correlation distance") between all possible paired combinations of the corresponding eigenvalues (or magnitudes) of the first three principal components. All paired combinations with a $D_{\text{corr}} < 0.15$ were considered as being part of the same group of correlation (Supplemental Fig. S2). Finally, each single-cell Ca^{2+} dynamics was sorted according to the identified groups of correlation and plotted against its position on the SST preparation.

Drugs Applied

Niquel (Ni^{2+}), mibefradil, T (Sigma-Aldrich), and thapsigargin (Alomone) were applied on the perfusion system during recordings, and 18 α -glycyrhethinic acid (Sigma-Aldrich) was incubated during 10 min between control and experimental condition. A 3 \times concentration of KCl (J.T. Baker) was applied (200 μl) into the bath using a pipette; the final concentration of KCl was 120 mM into the chamber recording. The final Ca^{2+} concentration present in Ringer without added Ca^{2+} was determined using Fura-2 and was between 0.5 and 1 μM .

RESULTS

SST Preparation

Acute tissue slices allow functional studies of several organs such as brain, cerebellum, adrenal medullae, and pituitary gland. Their use is adequate for examining functional multicellular networks and interactions between neighboring cells, a phenomenon that cannot be observed when cells are dissociated [21]. Technical approaches to obtain slices depend on the natural firmness of each particular tissue, as tissues have to be mounted on the plate of a vibratome and/or embedded in

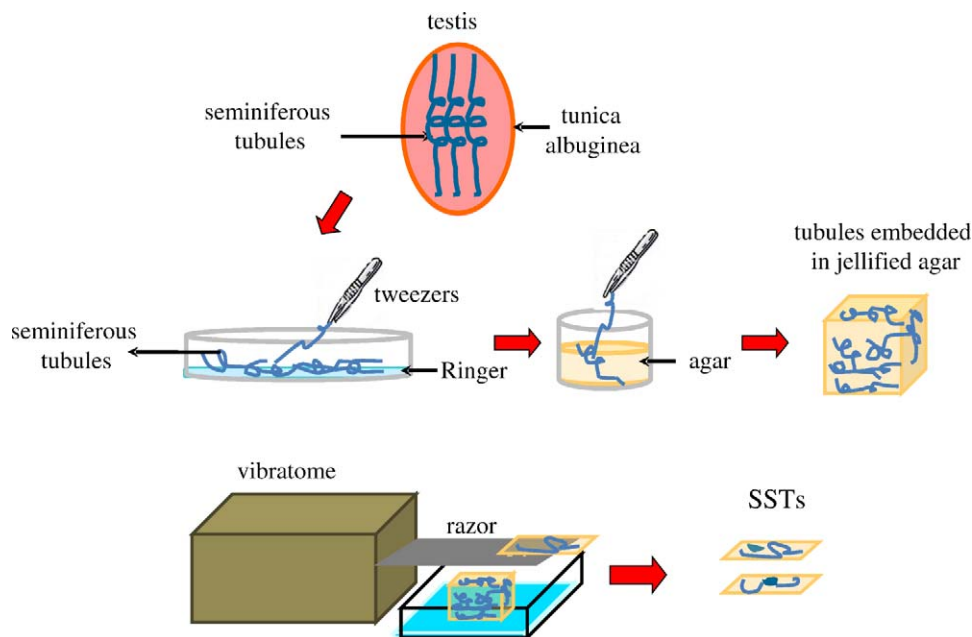


FIG. 1. Seminiferous tubule slice technique. Cartoon showing the methodological procedures followed for obtaining SSTs. Once the tunica albuginea is removed from mice testis, seminiferous tubules are mechanically dispersed with tweezers in a Petri dish containing Ringer solution and the dispersed tubules are embedded in agar. The agar cube is mounted on the plate of a vibratome where 160- μm -thick slices are obtained.

agar, as is the case for very soft tissues, to obtain mechanical stability during cutting. In this work we implemented for the first time the SST preparation from mouse testis. Figure 1 illustrates the procedure used (see *Materials and Methods*).

Seminiferous Tubules Slices Partially Retain the Tissue Structure

Seminiferous tubules were cut in several orientations, but for this study we used SSTs cut in a transversal orientation, that is, where the lumen of the seminiferous tubules can be identified. Histological transverse sections from seminiferous tubules (kindly provided by Diana Millán, Department of Cognitive Neuroscience, Institute of Cellular Physiology, UNAM, Mexico) established an anatomical reference to understand the distribution of germ cells in the freshly cut tubules. Accordingly, more differentiated germ cells are closer to the lumen and less differentiated cells are found towards the basal lamina of the seminiferous tubules. However, as shown in Figure 2B', in the transversal SST preparation it is not always possible to identify the typical anatomical distribution of germ cells or Sertoli cells, as mentioned above. Figure 2 illustrates different SSTs loaded with fluo-4AM and viewed under phase contrast microscopy (left panels) and fluorescence microscopy (right panels), at different magnifications. Images correspond to 10 \times (Fig. 2, A and A'), 20 \times (Fig. 2, B and B'), and 40 \times (Fig. 2, C and C') magnifications.

Germ Cells Are Viable and Display Spontaneous Ca^{2+} Oscillations in the SST

Given the anatomical complexity of the SST preparation, it is convenient to mention that for the selection of germ cells in the analysis of our experiments we used criteria such as cell size and shape: the size of round and condensing spermatids is between 8 and 10 μm and they are spherical and elongated respectively, whereas pachytene spermatocytes are spherical and 12–16 μm in size [35]; these parameters were used with the purpose of evaluating the responses of germ cells exclusively. In this regard, it should be mentioned that only 3% of the cell

population in the adult SST corresponds to Sertoli cells [35]. Thus it is reasonable to assume that the analysis performed in this study corresponds preponderantly to the activity of male germ cells.

Manipulation and cutting of seminiferous tubules during slice processing could damage germ cells. To test for germ cell viability in the slice, we used two strategies. First, we applied thapsigargin, an ATPase blocker; this drug raises $[\text{Ca}^{2+}]_i$ by preventing the cell from pumping Ca^{2+} into the endoplasmic reticulum, causing store depletion. Figure 3A shows that spermatogenic cells responded to thapsigargin application (10 μM) with a sustained $[\text{Ca}^{2+}]_i$ rise. Thapsigargin promoted a $[\text{Ca}^{2+}]_i$ increase in $87.3\% \pm 2.7\%$ of cells analyzed ($n = 4$ slices, 68 cells). Next, we used a membrane depolarization protocol, which consists in the application of saline containing 120 mM KCl into the bath. This procedure is useful to test the viability of cells because it opens Ca_v3 channels and/or other voltage-dependent channels and increases the $[\text{Ca}^{2+}]_i$. This treatment induced a transient $[\text{Ca}^{2+}]_i$ increase in $88.1\% \pm 2.4\%$ of the germ cells studied ($n = 4$ slices, 48 cells; Fig. 3B). These results suggest that the spermatogenic cells remain in a suitable physiological condition in the SST preparation.

Other cell types, such as neurons and endocrine cells, display spontaneous $[\text{Ca}^{2+}]_i$ oscillations under basal, resting conditions. Oscillations are rhythmic cytoplasmic Ca^{2+} transients that in some tissues are related to secretion (reviewed in [17, 36]). In Lymphocyte T cells, Ca^{2+} oscillations have been related to transcription regulation [37]. The occurrence of $[\text{Ca}^{2+}]_i$ oscillations has not been explored in germ cells before. To evaluate the presence of spontaneous $[\text{Ca}^{2+}]_i$ fluctuations in spermatogenic cells, we conducted long-lasting (10 min) Ca^{2+} imaging protocols under nonstimulated conditions (baseline recordings). Interestingly, approximately $65\% \pm 6.8\%$ of the germ cells analyzed ($n = 10$ slices, 386 cells) in SSTs displayed spontaneous Ca^{2+} oscillations of different frequency and amplitude (Fig. 3C); an example of this activity is shown in Supplemental Movie S1. To detect spontaneous Ca^{2+} fluctuations in several germ cells, we used a macro designed to plot fluorescence intensity changes corresponding to $[\text{Ca}^{2+}]_i$ varia-

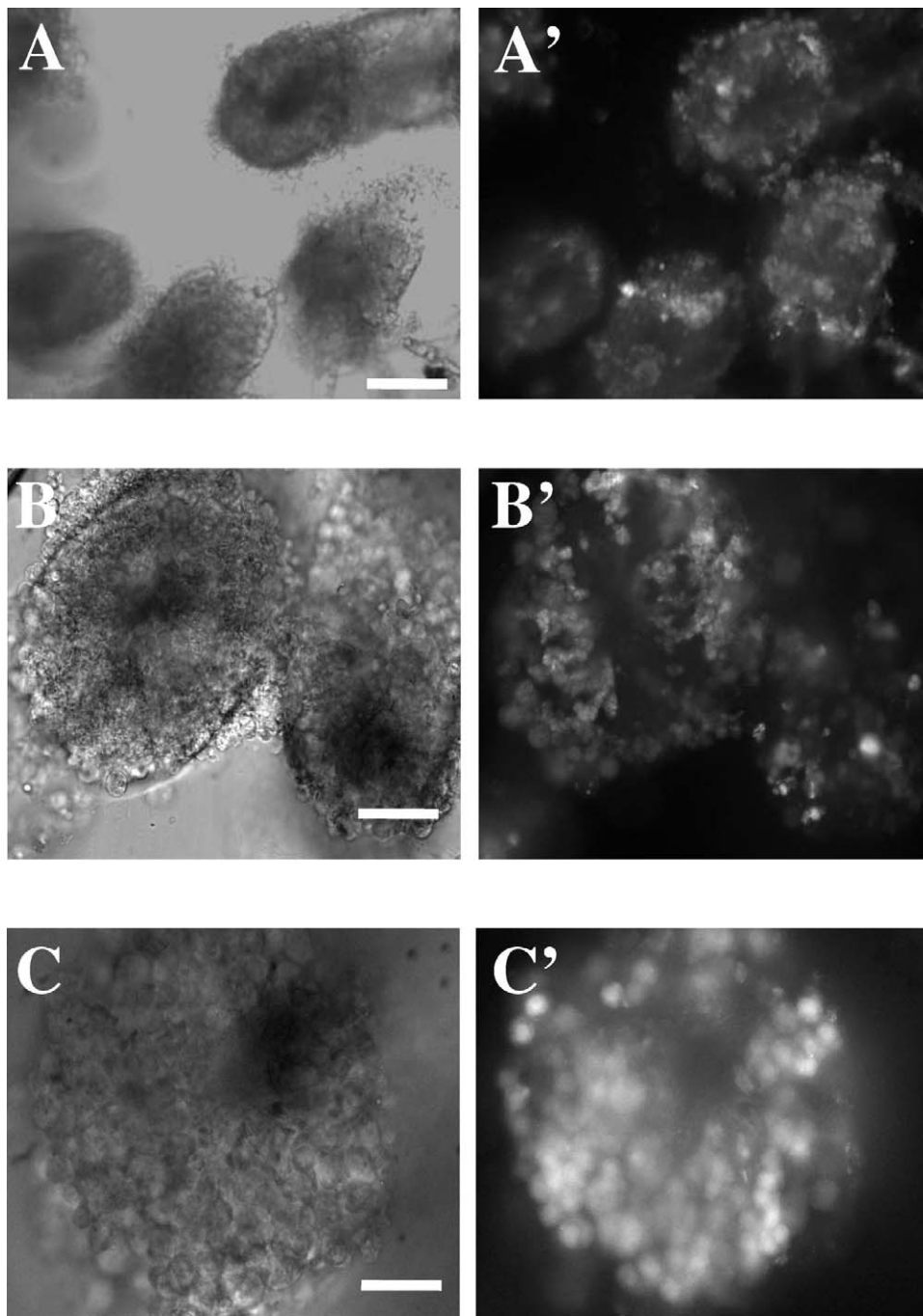


FIG. 2. Images of seminiferous tubule slices obtained at different magnifications. **A–C**) Three SSTs observed with phase contrast microscopy at $\times 10$, $\times 20$, and $\times 40$ magnifications. **A'–C'**) Fluorescence images of the same SST fields after incubation with fluo-4AM. In all images the seminiferous tubules were cut transversally. Bars (top to bottom) = 160, 80, and 40 μm .

tions of dozens of individual cells. These plots allowed us to identify germ cells displaying spontaneous $[\text{Ca}^{2+}]_i$ changes (Fig. 3D). In some cases these spontaneous $[\text{Ca}^{2+}]_i$ fluctuations occurred simultaneously in several germ cells (see below).

Spontaneous Ca^{2+} Oscillations Are Dependent on Extracellular Ca^{2+} and Are Partially Inhibited by Ca_v3 Blockers

Given that rodent germ cells express Ca_v3 channels, which allow the entry of extracellular Ca^{2+} into the cytoplasm of cells [12, 15], we decided to explore the possible participation of

these channels in the spontaneous Ca^{2+} oscillations displayed by germ cells in the SST. Recordings were made first for 10 min in a physiological solution containing 2 mM Ca^{2+} , and then the saline was switched for a solution containing no added CaCl_2 during 10 min (Fig. 4A, middle panel). Finally, the slice was perfused again with physiological saline with 2 mM external Ca^{2+} and the recording continued for 10 more min. The multicell plot (Fig. 4A) shows fluorescence fluctuations corresponding to Ca^{2+} oscillations displayed under basal conditions by more than 30 individual germ cells in an SST. These spontaneous Ca^{2+} fluctuations were practically abolished when the physiological solution was replaced with the

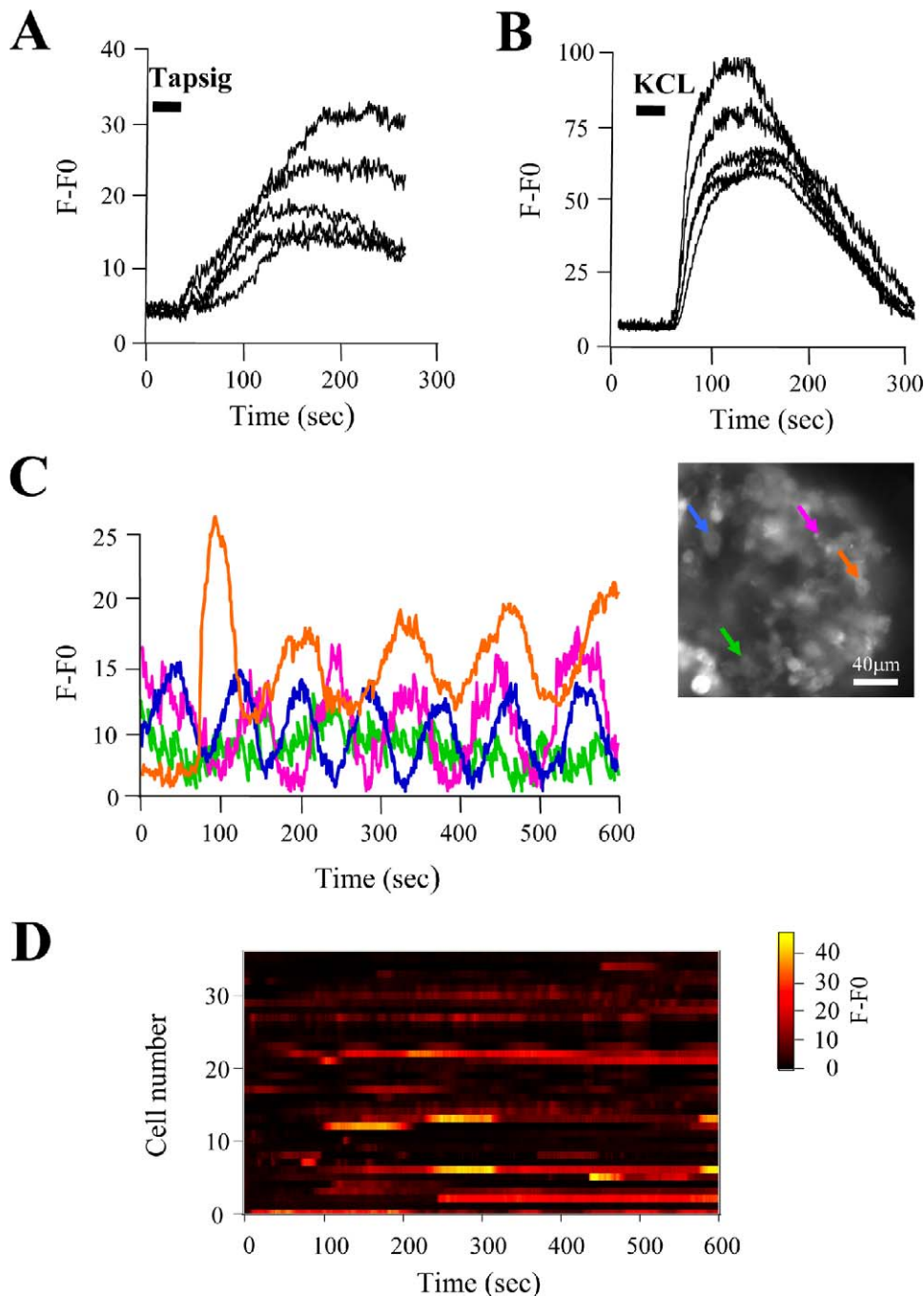


FIG. 3. Germ cells are viable in the SST and display spontaneous Ca^{2+} oscillations. Ca^{2+} recordings from germ cells in the SST corresponding to the addition of $10 \mu\text{M}$ thapsigargin (A) or 120 mM KCl (B). C) Fluorescence traces obtained from the four cells indicated by colored arrows in the still image (right) from Supplemental Movie S1 (for illustrative purposes the movie was reduced to show one frame every 10 sec and was accelerated to 10 frames per second). Germ cells displayed spontaneous Ca^{2+} fluctuations. D) Multicell plot showing fluorescence changes in pseudocolor scale corresponding to spontaneous Ca^{2+} oscillations obtained from 34 germ cells in an SST during 10 min of recording.

solution without added Ca^{2+} . This behavior was observed on $81\% \pm 9.7\%$ of the analyzed cells ($n = 4235$ cells). Restitution to normal 2 mM external Ca^{2+} promoted partial recovery of spontaneous Ca^{2+} oscillations in $57.4\% \pm 5.0\%$ of cells. Figure 4B shows recordings corresponding to three individual cells from the multicell plot in Figure 4A. Altogether these results suggest that Ca^{2+} entry is at least partially responsible for the spontaneous Ca^{2+} oscillations on SST germ cells.

Considering that Ca_v3 is the main type of Ca^{2+} channel involved in Ca^{2+} entry into germ cells [12, 15], we

evaluated the effect of Ni^{2+} and mibefradil, two Ca_v3 channel blockers, on spontaneous $[\text{Ca}^{2+}]_i$ oscillations of SST germ cells. As shown in Figure 4C, the application of NiCl_2 reduces the amplitude of $[\text{Ca}^{2+}]_i$ oscillations in two out of the three cells shown. Figure 4D summarizes the reduction caused by Ni^{2+} ($200 \mu\text{M}$) and mibefradil ($10 \mu\text{M}$) in the area under the curve in a 10-min period of $[\text{Ca}^{2+}]_i$ oscillations: Ni^{2+} reduced the area under the curve significantly from 1754.5 ± 306.8 to 1145.9 ± 224.6 ($P < 0.01$), whereas mibefradil did not (control, 3256 ± 156 ,

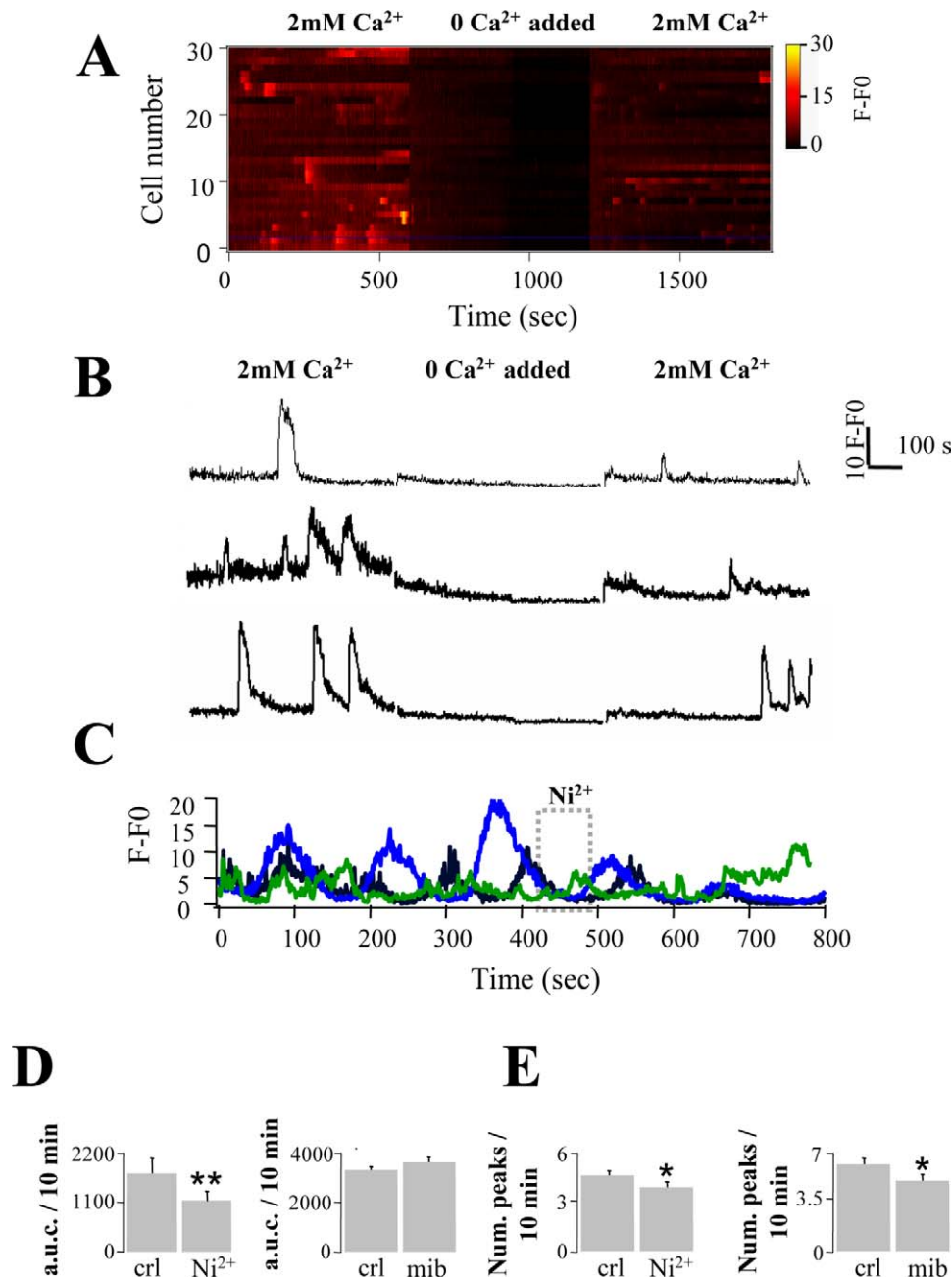


FIG. 4. Spontaneous Ca²⁺ oscillations are dependent on extracellular Ca²⁺ and are partially inhibited by a T type Ca²⁺ channel blocker. **A**) Multicell plot of spontaneous fluorescence changes in pseudocolor scale corresponding to Ca²⁺ fluctuations of germ cells in saline containing 2 mM Ca²⁺, no Ca²⁺ added, and 2 mM Ca²⁺ readdition. **B**) Individual Ca²⁺ recordings of three cells included in the multicell plot shown in **A**. In these cells the spontaneous Ca²⁺ fluctuations are completely abolished in the absence of extracellular Ca²⁺ and partially recovered after 2 mM Ca²⁺ addition. **C**) Ca²⁺ recordings of three cells displaying spontaneous Ca²⁺ oscillations. The amplitude of two of them is reduced after Ni²⁺ application. Quantitation of the Ni²⁺ and mibefradil (mib) effect on the area under the curve (**D**) and on the frequency (**E**) of spontaneous Ca²⁺ oscillations: asterisk denotes statistically significant differences, with **P* < 0.05 and ***P* = 0.001, using a Student *t*-test (*n* = 5 independent experiments for each condition).

vs. treatment, 3568 ± 256 , $P > 0.05$). However, when we evaluated the effect of the of Ca²⁺ channel blockers on the number of [Ca²⁺]_i fluctuations, we found that both Ni²⁺ and mibefradil diminished the frequency of [Ca²⁺]_i peaks recorded over a 10-min interval compared to the control (from 4.7 ± 0.26 to 3.98 ± 0.34 , $P < 0.05$, and 6.0 ± 0.40 to 4.9 ± 0.41 , $P < 0.05$, respectively). The differential effect observed with both Ca²⁺ channel blockers could be because of the fact that mibefradil has other targets in testis and sperm that include Catsper [38, 39] and K⁺ channels

[40]. Also, recently it has been shown that mibefradil can elevate basal [Ca²⁺]_i levels in human sperm [41].

Acutely Dissociated Germ Cells Also Display Spontaneous Ca²⁺ Oscillations

We then investigated if the Ca²⁺ oscillations were a property of germ cells in their natural environment inside the tubules or if they were also present in dissociated cells. For this purpose we conducted long-lasting Ca²⁺ imaging records from freshly dissociated germ cells loaded with fluo-4 AM (Fig.

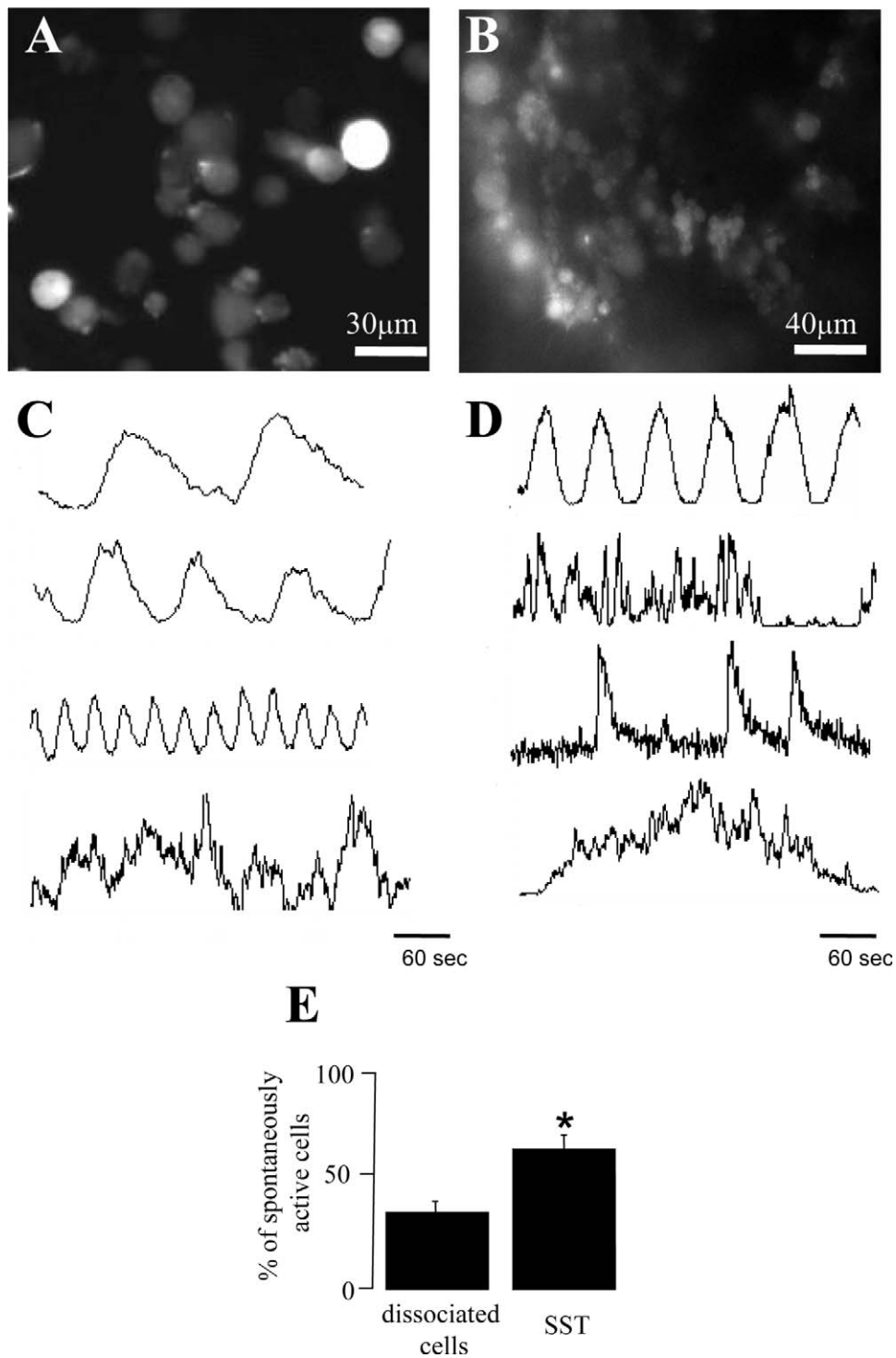


FIG. 5. Spontaneous Ca^{2+} fluctuation patterns are different in acutely dissociated germ cells and in SSTS. Fluorescence image obtained from freshly dissociated germ cells (see Supplemental Movie S2; the movie was reduced to show one frame every 10 sec and was accelerated to 10 frames per second) (A). Fluorescence image of germ cells in the SSTS preparation loaded with fluo-4 AM (B). Examples of spontaneous Ca^{2+} oscillations displayed by freshly dissociated germ cells (C) or by germ cells in an SSTS (D). Percentage of spontaneous Ca^{2+} fluctuations in germ cells freshly dissociated versus the SSTS preparation: asterisk denotes significant differences ($*P = 0.008$, Student *t*-test; dissociated germ cells: $n = 5$, 107 cells; SSTS: $n = 10$, 349 cells).

5A). The acquisition protocol was identical to the one applied for SSTS. We found that the majority of freshly dissociated germ cells also display spontaneous Ca^{2+} oscillations in a sinusoidal Ca^{2+} pattern ($79.66\% \pm 3.6\%$), although some ($20.34\% \pm 3.16\%$) cells showed other Ca^{2+} fluctuation patterns (see Supplemental Movie S2 and Fig. 5C). On the other hand, only $21\% \pm 7.7\%$ of germ cells in the SSTS

exhibited low-frequency Ca^{2+} oscillations with a sinusoidal pattern, similar to what is observed in freshly dissociated cells. Most germ cells in the SSTS ($78.9\% \pm 7.7\%$) displayed Ca^{2+} fluctuation patterns with complex frequency dynamics ($n = 10$ slices, 437 cells). Some of these complex patterns are illustrated in Figure 5D.

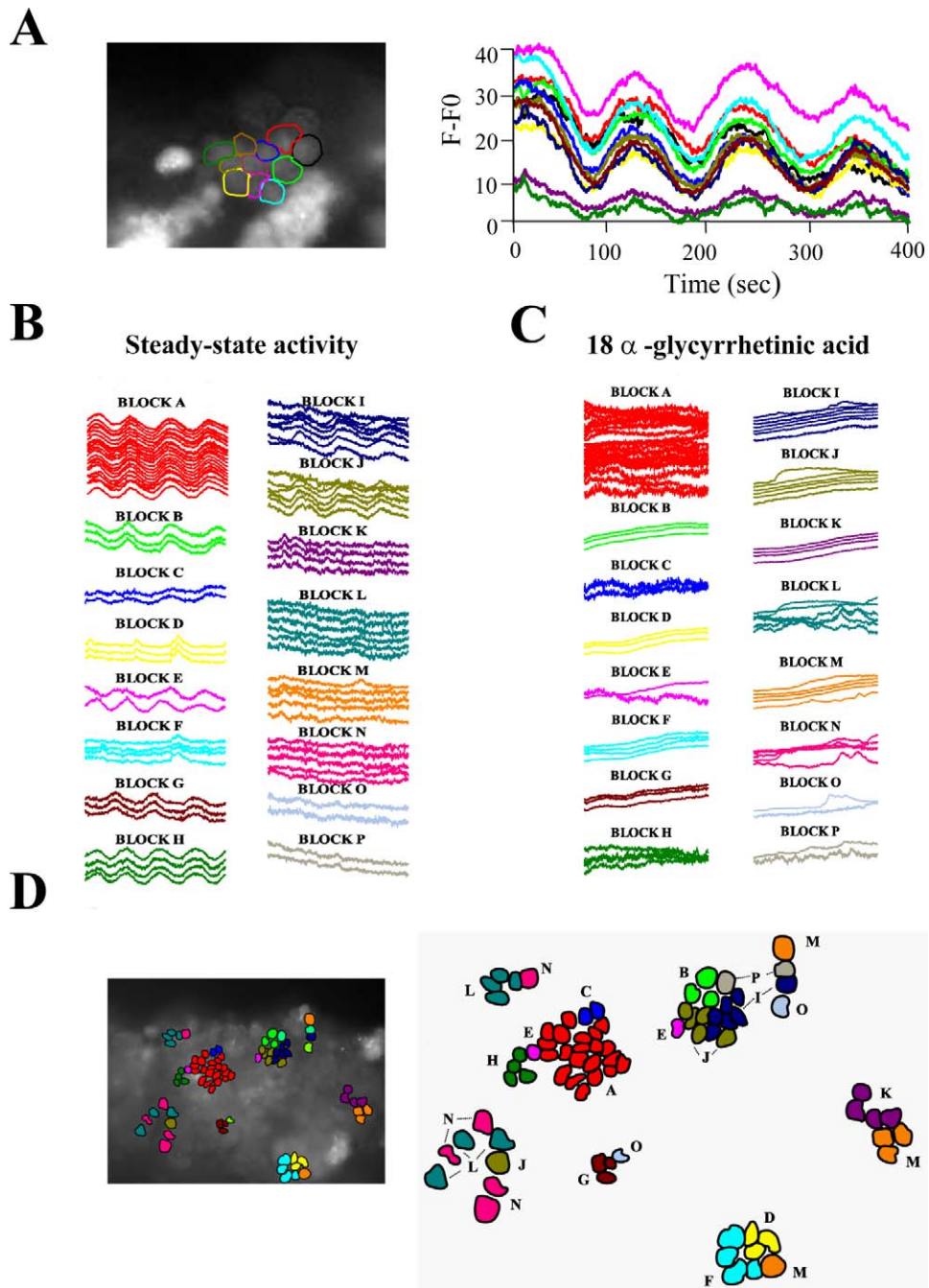


FIG. 6. Clustered germ cells in SST preparations display spontaneous coupled Ca^{2+} oscillations. **A**) Left, fluorescence image obtained from a cluster of germ cells displaying spontaneous, synchronized Ca^{2+} oscillations (see Supplemental Movie S3; the movie was reduced to show one frame every 10 sec and was accelerated to 10 frames per second). Right, color traces correspond to the individual Ca^{2+} recording of each cell indicated with a colored outline. **B**) Single Ca^{2+} time series of SST cells experiencing steady-state Ca^{2+} fluctuations classified according to the groups of correlation identified by PCA (see *Materials and Methods* and Supplemental Fig. S2). Each trace corresponds to the normalized fluorescence of an SST cell during 10 min. **C**) Selected regions occupied by cells displaying synchronous steady-state Ca^{2+} changes on an SST preparation. The inset shows a fluo-4 AM fluorescence image of an SST with the regions occupied by the selected cells. The color code is the same as in **A** and indicates the groups of correlation identified. **D**) Single Ca^{2+} time series of SST cells after treatment with AGA, organized and colored according to the groups of correlation identified in **B** showing alterations and/or uncoupling of Ca^{2+} oscillations.

To explore a possible correlation between Ca^{2+} oscillation patterns and the stage of germ cell differentiation, we identified three developmental stages in the SST: pachytene, round, and condensing spermatids. Nonetheless, after careful examination of the Ca^{2+} fluctuation patterns, we were unable to find a clear correlation among germ cell type and Ca^{2+} fluctuations (data not shown). Next, we compared if intact germ cells in the SST and freshly dissociated germ cells have the same propensity to

generate spontaneous Ca^{2+} oscillations. The results are shown in Figure 5E. As these graphs show, the percentage of germ cells showing spontaneous Ca^{2+} fluctuations is higher when cells are in the SST preparation ($65.5\% \pm 6.8\%$, $n = 10$ slices, 349 cells) than when cells are dissociated ($36.1\% \pm 4.5\%$, $n = 5107$ cells); differences are statistically significant ($P = 0.008$, t -test).

Spontaneous Ca^{2+} Oscillations Occur Synchronously in Clusters of Germ Cells

The anatomical and functional preservation of cells in the SST allowed recording some germ cells in clusters that displayed spontaneous synchronized Ca^{2+} fluctuations (see Fig. 6A). Next, we decided to mathematically evaluate the presence of “coupled” or synchronous spontaneous Ca^{2+} fluctuations between neighboring cells that has been observed in other tissues. To identify putative groups of cells displaying coupled steady-state Ca^{2+} fluctuations, a PCA was performed on all SST cells that presented spontaneous $[\text{Ca}^{2+}]_i$ oscillations. We selected 16 groups of correlation based on a correlation distance $D_{\text{cor}} < 0.15$ (their spatial proximity on a correlation space defined by the three principal components (PC1, PC2, and PC3; Supplemental Fig. S1A). Single cell $[\text{Ca}^{2+}]_i$ recordings were organized according to the groups identified (Fig. 6B), and mapped to their physical loci on the SST preparation (Fig. 6C). Interestingly, the cells that showed coupled Ca^{2+} activity are depicted as blocks of correlation in Figure 6, B and C. Figure 7A shows the physical distance on the SST preparation plotted against the correlation distance D_{cor} between single pairs of cells experiencing coupled Ca^{2+} fluctuations (black dots) or uncoupled Ca^{2+} fluctuations (white dots). The cells showing coupled Ca^{2+} fluctuations were closer in the SST preparation than the uncoupled cells ($P < 0.001$, Wilcoxon test). Similar results were obtained with at least three independent SST preparations (data not shown).

In summary, PCA analysis of spontaneous Ca^{2+} oscillations of SST germ cells reveals coupling of Ca^{2+} dynamics between clustered cells in physical contact, as shown in Supplemental Movie S3, suggesting functional coupling via local communication.

A GJ Blocker Uncouples the Ca^{2+} Fluctuations of SST Germ Cell Clusters

In the seminiferous tubules, interacting Sertoli-Sertoli and Sertoli-germ cells express functional GJs [28, 42]. The blocker AGA has been used to suppress electrical coupling between neighboring cells. This compound also decreases the diffusion of a fluorescent dye in the seminiferous tubules due to GJ coupling [29]. We used AGA to investigate if the synchronization of Ca^{2+} fluctuations observed is mediated by GJs. An SST preparation displaying synchronization of Ca^{2+} fluctuations (as described earlier) was incubated with 10 μM AGA during 10 min. PCA analysis revealed that some of the clusters identified prior to treatment became uncoupled after AGA treatment (compare Supplemental Fig. S2, A and B, and Fig. 6, B and D, blocks A, C, E, H, L, and N–P). However, other SST cells showed a steady $[\text{Ca}^{2+}]_i$ rise and a false “coupling” following AGA treatment, probably reflecting impairment of Ca^{2+} homeostasis in neighboring germ cells (Fig. 6D, blocks B, D, F, G, I–K, and M). The SST cells whose $[\text{Ca}^{2+}]_i$ increased steadily over time formed a new group of correlation (Fig. S1B; Fig. 6D, blocks B, D, F, G, I–K, and M). The plot of the physical distance (d) against D_{cor} between single pairs of SST clustered cells showed that some of them missed their synchronous Ca^{2+} fluctuations but, obviously, not their physical proximity (Fig. 6D, blocks A, C, E, H, L, and N–P; Fig. 7C). Some other SST cells remained coupled (Fig. 7C) but exhibited different Ca^{2+} dynamics (Fig. 6D, blocks B, D, F, G, I–K, and M). However, the overall Ca^{2+} coupling between germ cells in the SST was impaired by AGA: their overall intragroup correlation distance increased (compare Figs. 7B and 6D, left; $P < 0.001$, Wilcoxon test), but not their physical proximity (Fig. 7, B and D, right).

T Promotes an Increase in $[\text{Ca}^{2+}]_i$ in Some Cells in the SST

T is a hormone crucial for spermatogenesis that exerts its effects indirectly via an androgen receptor localized in Sertoli cells (reviewed in [43]). These cells are essential for the maintenance and development of spermatogenesis, because they give support and nutrition to germ cells. Sertoli cells are coupled to each other by GJs and this coupling is fundamental for spermatogenesis. Considering that the SST preparation allows partial conservation of the tissue architecture, we explored the possibility of identifying functional Sertoli cells in our preparation by looking at their specific Ca^{2+} signals. Previous studies using freshly dissociated Sertoli cells and primary culture of seminiferous tubules reported that nanomolar concentrations of T promote $[\text{Ca}^{2+}]_i$ elevations in Sertoli cells [5, 44]. Germ cells and Sertoli cells are intermingled, which makes the identification of the latter difficult in our preparation. For this reason, and taking advantage of the fact that the expression of T receptors is low in germ cells [45], we applied this hormone to SSTs during Ca^{2+} recordings to try to identify Sertoli cells. In three of these experiments we were able to detect elongated cells intermingled with germ cells, an anatomical characteristic compatible with Sertoli cells, which responded to T (100 nM) application with a $[\text{Ca}^{2+}]_i$ increase. An example of the response of one of these cells is shown in Figure 8A and Supplemental Movie S4. Here, the red arrows indicate a cytoplasmic prolongation of a putative Sertoli cell located between three germ cells. Figure 8B shows a sequence of fluorescence images obtained after T application: the first panel exemplifies one cell (1) responding to T application with a Ca^{2+} increase (+T). In the second panel (15 sec later) the Ca^{2+} signal spreads to another two cells (2) probably corresponding to germ cells. After 60 sec, the Ca^{2+} signal propagates, apparently through cytoplasmic processes that could be part of Sertoli cells surrounding germ cells (3, 4). Finally, the last panel (275”) shows that Ca^{2+} signals from all participating cells in the field terminated. Figure 8C illustrates the individual Ca^{2+} responses promoted by T application to cells labeled 1–4 in Figure 8B. These records suggest that Ca^{2+} signals stimulated by this hormone are slow, transient, and initiated in Sertoli cells, then spread to other neighboring cells that could include both germ cells and other Sertoli cells.

DISCUSSION

Ca^{2+} oscillations are generated by periodic Ca^{2+} influx from the extracellular medium and/or Ca^{2+} release from intracellular Ca^{2+} stores. These Ca^{2+} increases result from the orchestrated activity of ion channels, transporters, and pumps on the plasma membrane and the ER, which coordinately regulate Ca^{2+} homeostasis in the cytoplasm of cells. Ca^{2+} oscillations are involved in the regulation of several cellular functions, including secretion, development, differentiation, and fertilization [46, 47]. Previous studies reported, not surprisingly, that male germ cells possess their own mechanisms to regulate cytoplasmic Ca^{2+} , which include voltage-gated Ca^{2+} channels and intracellular channels, InsP_3R and ryanodine receptors [9, 12, 15]. However, few studies report $[\text{Ca}^{2+}]_i$ dynamics in spermatogenic cells [16, 48–51]. In this work we implemented for the first time a technique that allows the study of $[\text{Ca}^{2+}]_i$ dynamics on dozens of germ cells in a context that preserves the architecture of the native tissue. We provide evidence that the spontaneous Ca^{2+} fluctuations in germ cells depend, at least in part, on Ca^{2+} entry through Ca_v3 channels. The Ca^{2+} oscillation patterns exhibited by freshly dissociated germ cells are different from those displayed by these cells in the acute SST preparation. Our results have demonstrated that spontaneous Ca^{2+} fluctuations in germ cells

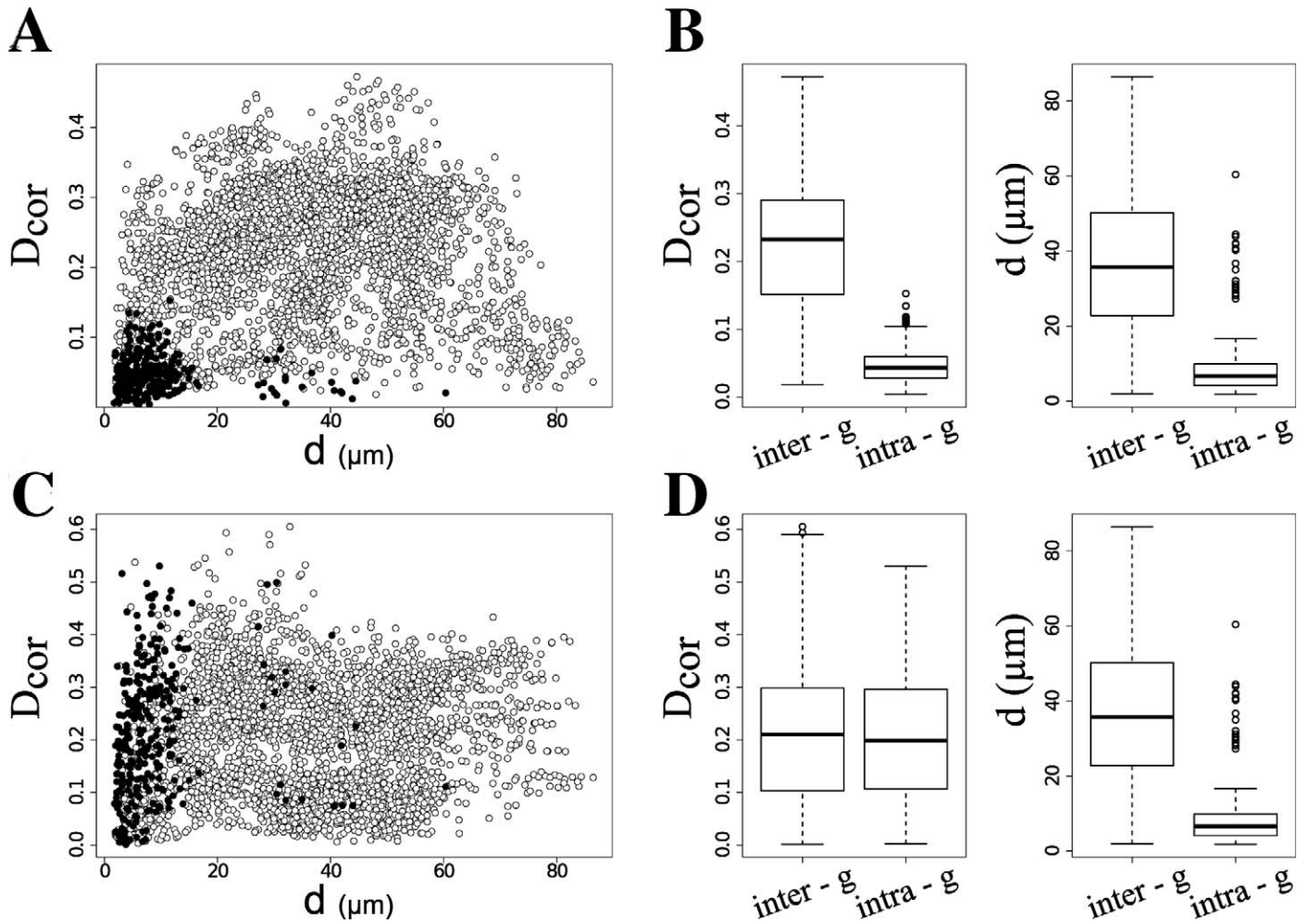


FIG. 7. A GJ blocker disrupts the Ca^{2+} activity coupling of SST germ cells. **A, C** Physical distance (d) on the SST against the correlation distance (D_{cor}) between single pairs of clustered cells (black dots), and between pairs of cells of different clusters (white dots) experiencing steady-state Ca^{2+} activity (**A**) and after exposure to AGA (**C**). **B, D** Overall correlation (left) and physical distance (right) between pairs of cells of different correlation clusters (intergroup distance), before (**B**) and after AGA treatment (**D**). Each box contains 50% of values, the inner lines indicate the median, and the error bars define 95% outliers.

can occur synchronously in clusters composed of up to 20–21 cells in the SST (Fig. 6B). These clusters display the Ca^{2+} oscillation pattern for long periods of time (at least 10 min). In contrast, other cells display asynchronous spontaneous Ca^{2+} oscillations never involving other cells during the recording. Our experiments suggest that GJs could be mediating the synchronization of spontaneous Ca^{2+} oscillations in germ cells. However, because the GJ blocker (AGA) affects synchronization in some clusters but not in others, additional mechanisms such as IBs should be invoked to explain the synchronization phenomena.

Additionally, the SST preparation allowed us to record Ca^{2+} responses stimulated by T application in cells that functionally and anatomically resemble Sertoli cells. All these findings indicate that SST is an ideal preparation to begin approaching the study of functional cell-cell interactions during germ cell differentiation in the testis seminiferous tubules.

Ca^{2+} oscillations in germ cells are involved in many important cell functions. The development and differentiation of oocytes in the ovary is a relevant example (reviewed in [52]). Immature oocytes display spontaneous Ca^{2+} oscillations [45], which are present in $\sim 70\%$ of oocytes released from the antral or preantral follicles [53, 54]. Notably, the presence of Ca^{2+} oscillations in male germ cells has not been previously

described. In this work we found that 65% of spermatogenic cells in SST generate spontaneous Ca^{2+} oscillations, whereas only 36% of dissociated cells do so. This could be an indication of cell damage or removal of cell-to-cell communication with neighboring cells during dissociation. Spermatogenic cells displayed regular and irregular spontaneous Ca^{2+} fluctuations ranging from 0.1 to 2 spikes/sec (60-fold more frequent than oocytes [53]). In oocytes, the patterns of spontaneous Ca^{2+} oscillations depend on the stage of oocyte maturation [53]. Nonetheless, we did not observe significant differences of Ca^{2+} oscillation patterns at different stages of spermatogenic cell maturation, at least in the developmental range from pachytene spermatocytes to condensing spermatids. Also, we observed a higher proportion (78.9%) of irregular signaling patterns in germ cells in the SST, which could indicate more complex Ca^{2+} signaling events, possibly due to interactions with different cells type in the tissue.

Ca^{2+} oscillations have been related to the control of gene expression during cell differentiation. An example of this was shown using microarray studies on cultured mouse cerebellar granular cells exposed to depolarized conditions. In this study, membrane potential depolarization, linked to Ca^{2+} entry, was related to the induction of many genes implicated in cell proliferation, differentiation, migration, and neurite growth of

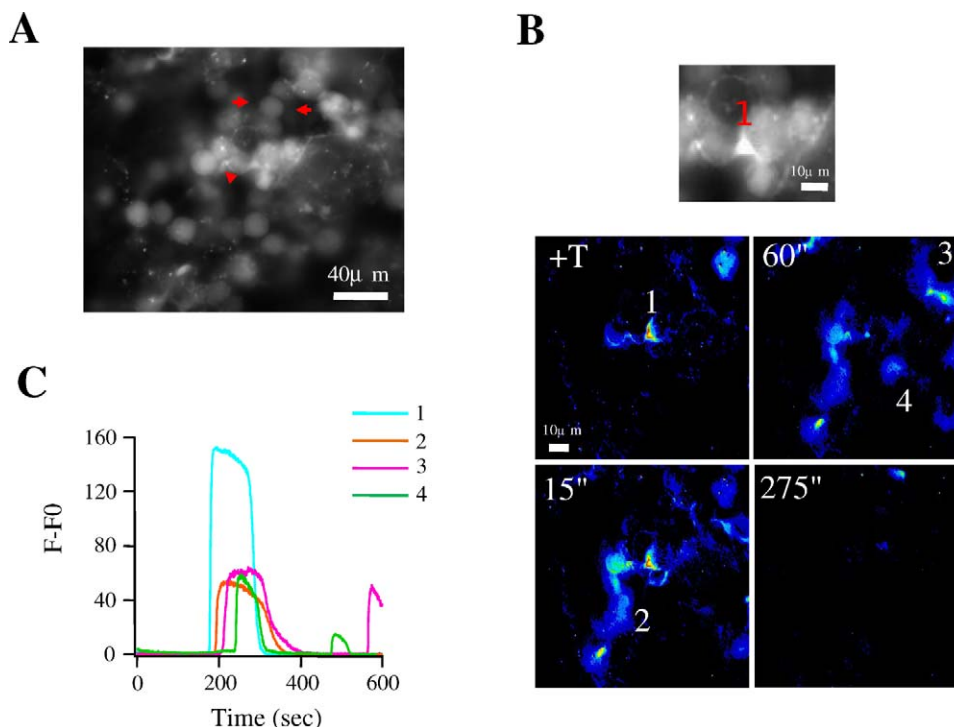


FIG. 8. T promotes Ca^{2+} responses in elongated cells into the SST. **A**) Fluorescence image of an SST. Elongated structures can be seen between germ cells (shown by red arrows). **B**) As shown in Supplemental Movie S4, T application (100 nM) promotes an immediate Ca^{2+} increase in one cell, illustrated in the upper panel (1), also shown in the first pseudocolored panel (+T); the response is propagated to other cells after 15 (15") and 60 sec (60"); the Ca^{2+} increase disappears on these cells after 275 sec (275") of T application. The movie was reduced to show one frame every 10 sec and was accelerated to 10 frames per second. **C**) Transitory Ca^{2+} responses promoted by T in cells 1, 3, and 4 in the pseudocolored images in **B**.

immature granule cells [55]. In oocytes it has also been shown that a $[\text{Ca}^{2+}]_i$ rise is important during differentiation by suppressing the meiotic arrest and leading to meiosis progress [56]. Although it is difficult to predict which role Ca^{2+} oscillations may have on germ cell physiology and development, their presence could impact gene regulation, transcription, and/or structural and functional regulation during spermatogenesis.

Several research groups have made technical efforts to mimic the native testis environment, using mainly variants of cellular cocultures to perform functional studies [57–59]. However, only the use of testis organ culture has recently allowed the successful development of mammalian spermatogenesis in vitro [60], indicating that good tissue preservation is fundamental for appropriate male germ cell differentiation and maturation. Interestingly, we observed that spontaneous Ca^{2+} oscillations in male germ cells occur synchronously in the SST preparation, suggesting that functional cell-cell communication is important during spermatogenesis. The effect of AGA on spontaneous Ca^{2+} oscillations is consistent with the participation of GJs in spermatogenic cell coupling. This result is in agreement with immunodetection of connexin 43 in spermatogenic cells [40]. The IBs are evolutionarily conserved and allow cytoplasm sharing among spermatogenic cells during the synchronous cell divisions in the seminiferous tubules [30]. IBs are 1–3 μm in diameter [31] and form syncytial clusters resulting from incomplete cytokinesis. These IBs allow the movement of many cellular components, including cytoplasmic materials and even organelles [61]. Therefore, the free passage of Ca^{2+} ions is not difficult to imagine and could explain the presence of functional clusters displaying synchronous Ca^{2+} oscillations, as we observed in this study. Electron microscopy reports in rodent germ cells have detected syncytia composed

of 2–100 spermatogenic cells [62]. In our study, we demonstrated synchronous Ca^{2+} fluctuations in clusters composed of 2–21 cells. Perhaps we are unable to detect larger clusters simply because the fluorescence signal is collected from a focal plane in the tissue, and we could be missing information from cluster members deeper into the SST. Three-dimensional confocal microscopy may represent an alternative to circumvent this limitation [63]. Also, it is possible that not all spermatogenic cells from a cluster display the same Ca^{2+} pattern. One can imagine that other elements, such as GJs or paracrine factors, could modify the spontaneous Ca^{2+} patterns of one part of the cluster, despite the presence of IBs. Thus, we believe that synchronous Ca^{2+} fluctuations in spermatogenic cells in the SST result from more than one mechanism, including GJs, IBs, or paracrine/autocrine factors. However, independently of the mechanism involved, given that germ cells joined by IBs exhibit synchronous differentiation [30], we hypothesize that Ca^{2+} diffusion through these structures could participate as a synchronization signal to regulate differentiation during spermatogenesis.

The results obtained in experiments using Ca^{2+} channel blockers suggest that these channels are at least one of the Ca^{2+} sources participating in the spontaneous Ca^{2+} oscillations of spermatogenic cells. These findings coincide with previous reports using electrophysiological [11, 15], immunocytochemical, and molecular techniques [8–10] suggesting the presence of Ca_v3 channels in spermatogenic cells. As shown here, Ca^{2+} oscillations are practically abolished in the absence of extracellular Ca^{2+} . However, we cannot rule out the possibility that Ca^{2+} release from intracellular Ca^{2+} stores mediated by ryanodine and InsP_3 receptors also participates in the generation of Ca^{2+} signals. In fact, the expression of these

intracellular receptors has been reported in spermatogenic cells [12, 16].

Spermatogenic tubules are composed mainly of germ and Sertoli cells. The developing germ cells are in close contact with Sertoli cells that nurture them and provide them with structural support. These Sertoli-spermatogenic cell contacts are crucial for spermatogenesis and involve both tight junctions and GJs [28, reviewed by 64]. Branches of Sertoli cell cytoplasm surround the differentiating spermatocytes and spermatids [65], forming a three-dimensional network through which spermatogenesis is modulated via paracrine factors, hormones, proteases, protease inhibitors, and components of the extracellular matrix produced by both Sertoli and germ cells (reviewed in [65]). The Ca^{2+} responses stimulated by application of T in the SST suggest that Sertoli cells remain functional in the slice, allowing the spreading of Ca^{2+} waves between networks of Sertoli cells possibly mediated through GJs.

In summary, we demonstrated that the SST is an excellent biological preparation to investigate germ cell function in vitro. In this preparation, intercellular connections remain functional and paracrine/autocrine interactions between the different cell types of the seminiferous tubules continue to take place. Unlike other preparations requiring 12–24 h of stabilization and recovery, the SST preparation allows physiological recordings within 1 h after dissection. This should be relevant if one attempts to preserve physiological responses as reliably as possible. The spontaneous Ca^{2+} oscillations displayed by spermatogenic cell clusters in the SST attest to their viability and functional state. We believe that SST is a preparation with great potential for future studies on the role of orchestrated $[\text{Ca}^{2+}]_i$ changes in spermatogenesis.

ACKNOWLEDGMENT

We are grateful to Dr. León Islas for writing Igor-Pro algorithms and to Jorge Carneiro for his comments on the PCA analysis. We also express our gratitude to Jose Luis De la Vega, Yoloxóchtitl Sánchez, Shirley Ainsworth, Elizabeth Mata, Marcela Ramírez, Nicolás Jiménez, Diana Millán, and Claudia V. Rivera-Cerecedo for their excellent technical support.

REFERENCES

- Holdcraft RW, Braun RE. Hormonal regulation of spermatogenesis. *Int J Androl* 2004; 27:335–342.
- Mruk DD, Cheng CY. Sertoli-Sertoli and Sertoli-germ cell interactions and their significance in germ cell movement in the seminiferous epithelium during spermatogenesis. *Endocr Rev* 2004; 25:747–806.
- Syed V, Hecht NB. Disruption of germ cell-Sertoli cell interactions leads to spermatogenic defects. *Mol Cell Endocrinol* 2002; 186:155–157.
- Berridge MJ, Bootman MD, Roderick HL. Calcium signalling: dynamics, homeostasis and remodelling. *Nat Rev Mol Cell Biol* 2003; 4:517–529.
- Gorzynska E, Handelsman DJ. Androgens rapidly increase the cytosolic calcium concentration in Sertoli cells. *Endocrinology* 1995; 136:2052–2059.
- Gorzynska E, Handelsman DJ. The role of calcium in follicle-stimulating hormone signal transduction in Sertoli cells. *J Biol Chem* 1991; 266:23739–23744.
- Loss ES, Jacobus AP, Wassermann GF. Diverse FSH and testosterone signaling pathways in the Sertoli cell. *Horm Metab Res* 2007; 39:806–812.
- Tovey SC, Godfrey RE, Hughes PJ, Mezna M, Minchin D, Mikoshiba K, Michelangeli F. Identification and characterization of inositol 1,4,5-trisphosphate receptors in rat testis. *Cell Calcium* 1997; 21:311–319.
- Treviño CL, Santi CM, Beltrán C, Hernández-Cruz A, Darszon A, Lomeli H. Localisation of inositol trisphosphate and ryanodine receptors during mouse spermatogenesis: possible functional implications. *Zygote* 1998; 6:159–172.
- Chiarella P, Puglisi R, Sorrentino V, Boitani C, Stefanini M. Ryanodine receptors are expressed and functionally active in mouse spermatogenic cells and their inhibition interferes with spermatogonial differentiation. *J Cell Sci* 2004; 117:4127–4134.
- Arnoult C, Villaz M, Florman HM. Pharmacological properties of the T-type Ca^{2+} current of mouse spermatogenic cells. *Mol. Pharmacol* 1998; 53:1104–1111.
- Treviño CL, Felix R, Castellano LE, Gutierrez C, Rodriguez D, Pacheco J, Lopez-Gonzalez I, Gomora JC, Tsutsumi V, Hernandez-Cruz A, Fiordelisio T, Scaling AL, Darszon A. Expression and differential cell distribution of low-threshold Ca^{2+} channels in mammalian male germ cells and sperm. *FEBS Lett* 2004; 563:87–92.
- Darszon A, Nishigaki T, Beltrán C, Treviño CL. Calcium channels in the development, maturation and function of spermatozoa. *Physiol Rev* 2011; 91:1305–1355.
- Benoff S. Voltage dependent calcium channels in mammalian spermatozoa. *Front Biosci* 1998; 3:D1220–1240.
- Liévano A, Santi CM, Serrano CJ, Treviño CL, Bellvé AR, Hernández-Cruz A, Darszon A. T-type Ca^{2+} channels and $\alpha 1E$ expression in spermatogenic cells, and their possible relevance to the sperm acrosome reaction. *FEBS Lett* 1996; 388:150–154.
- Berrios J, Osses N, Opazo C, Arenas G, Mercado L, Benos DJ, Reyes JG. Intracellular Ca^{2+} homeostasis in rat rous spermatids. *Biol Cell* 1998; 90:391–398.
- Stojilkovic SS. Pituitary cell type-specific electrical activity, calcium signaling and secretion. *Biol Res* 2006; 39:403–23.
- Hellman B, Gylfe E, Grapengiesser E, Lund PE, Berts A. Cytoplasmic Ca^{2+} oscillations in pancreatic beta-cells. *Biochim Biophys Acta* 1992; 1113:295–305.
- Malgaroli A, Meldolesi J. $[\text{Ca}^{2+}]_i$ oscillations from internal stores sustain exocytotic secretion from the chromaffin cells of rat. *FEBS Lett* 1991; 283:169–172.
- Van Goor F, Zivadinovic D, Martinez-Fuentes AJ, Stojilkovic SS. Dependence of pituitary hormone secretion on the pattern of spontaneous voltage-gated calcium influx. Cell type-specific action potential secretion coupling. *J Biol Chem* 2001; 276:33840–33846.
- Bonnefont X, Lacampagne A, Sanchez-Hornigó A, Fino E, Creff A, Mathieu MN, Smallwood S, Carmignac D, Fontanaud P, Travo P, Alonso G, Courtois-Coutry N, et al. Revealing the large-scale network organization of growth hormone-secreting cells. *Proc Natl Acad Sci U S A* 2005; 102:16880–16885.
- Siu MK, Cheng CY. Extracellular matrix: recent advances on its role in junction dynamics in the seminiferous epithelium during spermatogenesis. *Biol Reprod* 2004; 71:375–391.
- Mruk DD, Cheng CY. Tight junctions in the testis: new perspectives. *Philos Trans R Soc Lond B Biol Sci* 2010; 365:1621–1635.
- Saez JC, Berthoud VM, Branes MC, Martinez, AD, Beyer EC. Plasma membrane channels formed by connexins: their regulation and functions. *Physiol Rev* 2003; 83:1359–1400.
- Harris AL. Connexin channel permeability to cytoplasmic molecules. *Prog Biophys Mol Biol* 2007; 94:120–143.
- Batias C, Siffroi JP, Fénichel P, Pintis G, Segretain D. Connexin 43 gene expression and regulation in the rodent seminiferous epithelium. *J Histochem Cytochem* 2000; 48:793–805.
- Bravo-Moreno JF, Díaz-Sánchez V, Montoya-Flores JG, Lamoyi E, Saéñz CJ, Pérez-Armendáriz ME. Expression of connexin43 in mouse Leydig, Sertoli, and germinal cells at different stages of postnatal development. *Anat Rec* 2001; 264:13–24.
- Decrouy X, Gasc JM, Pointis G, Segretain D. Functional characterization based gap junctions during spermatogenesis. *J Cell Physiol* 2004; 200:146–154.
- Gilleron J, Carette D, Durand P, Pointis G, Segretain D. Connexin 43 a potential regulator of cell proliferation and apoptosis within the seminiferous epithelium. *Int J Biochem Cell Biol* 2009; 41:1381–1390.
- Fawcett DW, Ito S, Slautterback D. The occurrence of intercellular bridges in groups of cells exhibiting synchronous differentiation. *J Biophys Biochem Cytol* 1959; 5:453–60.
- Dym M, Fawcett DW. Further observations on the numbers of spermatogonia, spermatocytes and spermatids connected by intercellular bridges in the mammalian testis. *Biol Reprod* 1971; 4:195–215.
- Hermo L, Pelletier RM, Cyr DG, Smith CE. Surfing the wave, cycle, life history, and genes/proteins expressed by testicular germ cells. Part 4: intercellular bridges, mitochondria, nuclear envelope, apoptosis, ubiquitination, membrane/voltage-gated channels methylation/acetylation, and transcription factors. *Microsc Res Tech* 2010; 73:364–408.
- R Development Core Team. R: A Language and Environment for Statistical Computing. Vienna, Austria: R Foundation for Statistical Computing; 2010. <http://www.r-project.org/>.
- Jolliffe IT. *Principal Component Analysis*, 2nd ed. Springer Series in Statistics. New York: Springer; 2002:487.

35. Bellvé AR. Purification, culture, and fractionation of spermatogenic cells. *Methods Enzymol* 1993; 225:84–113.
36. Low JT, Shukla A, Thorn P. Pancreatic acinar cell: new insights into the control of secretion. *Int J Biochem Cell Biol* 2010; 42:1586–1589.
37. Dolmetsch RE, Xu K, Lewis RS. Calcium oscillations increase the efficiency and specificity of gene expression. *Nature* 1998; 392:933–936.
38. Quill TA, Ren D, Clapham DE, Garbers DL. A voltage-gated ion channel expressed specifically in spermatozoa. *Proc Natl Acad Sci USA* 2001; 98:12527–12531.
39. Jin JL, O'Doherty AM, Wang S, Zheng S, Sanders KM, Yan W. Catsper 3 and Catsper 4 encode two cation channel-like proteins exclusively expressed in testis. *Biol Reprod* 2005; 73:1235–1242.
40. Navarro B, Kirichok Y, Clapham DE. KSper, a pH sensitive K⁺ current that controls sperm membrane potential. *Proc Natl Acad Sci USA* 2007; 104:7688–7692.
41. Torres Flores-V, Picaso-Juárez G, Hernández-Rueda Y, Darszon A, Gonzalez-Martínez MT. Sodium influx induced by external calcium chelation decreases human sperm motility. *Hum Reprod*. 2011; 26:2626–2635.
42. Risley MS, Tan IP, Roy C, Sáenz JC. Cell-, age- and stage-dependent distribution of connexin 43 gap junctions in testes. *J Cell Sci* 1992; 103:81–96.
43. Silva FR, Leite LD, Wasseermann GF. Rapid signal transduction in Sertoli cells. *Eur J Endocrinol* 2002; 147:425–433.
44. Lying FM, Jones GR, Rommerts FF. Rapid androgen actions on calcium signaling in rat Sertoli cells and two human prostatic cell lines similar biphasic responses between 1 picomolar and 100 nanomolar concentrations. *Biol Reprod* 2000; 63:736–47.
45. Bremner WJ, Millar MR, Sharpe RM, Saunders PT. Immunohistochemical localization of androgen receptors in the rat testis: evidence for stage-dependent expression and regulation by androgens. *Endocrinology* 1994; 135:1227–34.
46. Carroll J, Swann K. Spontaneous cytosolic calcium oscillations driven by inositol trisphosphate occur during in vitro maturation of mouse oocytes. *J Biol Chem* 1992; 267:11196–11201.
47. Tengholm A, Gylfe E. Oscillatory control of insulin secretion. *Mol Cell Endocrinol* 2009; 297:58–72.
48. Reyes JG, Herrera E, Lobos L, Salas K, Lagos N, Jorquera RA, Labarca P, Benos DJ. Dynamics of intracellular calcium induced by lactate and glucose in rat pachytene spermatocytes and round spermatids. *Reproduction* 2002; 123:701–710.
49. Mishra DP, Pal R, Shaha C. Changes in cytosolic Ca²⁺ levels regulate BCL-xS and Bcl-xL expression in spermatogenic cells during apoptotic death. *J Biol Chem* 2006; 281:2133–2143.
50. Treviño CL, De la Vega-Beltrán JL, Nishigaki T, Felix R, Darszon A. Maitotoxin potently promotes Ca²⁺ influx in mouse spermatogenic cells and sperm, and induces the acrosome reaction. *J Cell Physiol* 2006; 206:449–456.
51. Reyes JG, Osses N, Knox M, Darszon A, Treviño CL. Glucose and lactate regulate maitotoxin-activated Ca²⁺ entry in spermatogenic cells: the role of intracellular [Ca²⁺]. *FEBS Lett* 2010; 584:3111–3115.
52. Ducibella T, Fissore R. The roles of Ca²⁺, downstream protein kinases, and oscillatory signaling in regulating fertilization and the activation of development. *Dev Biol* 2008; 315:257–279.
53. Carroll J, Swann K, Whittingham D, Whitaker M. Spatiotemporal dynamics of intracellular [Ca²⁺]_i oscillations during the growth and meiotic maturation of mouse oocytes. *Development* 1994; 120:3507–3517.
54. Gomes JE, Pesty A, Gouveia-Oliveira A, Cidadao AJ, Plancha CE, Lefèvre B. Age and gonadotropins control Ca²⁺-spike acquisition in mouse oocytes isolated from early preantral follicles. *Int J Dev Biol* 1999; 43:839–842.
55. Sato M, Suzuki K, Yamazaki H, Nakanishi S. A pivotal role of calcineurine signaling in development and maturation of postnatal cerebellar granule cells. *Proc Natl Acad Sci U S A* 2005; 102:5874–5879.
56. Boni R, Gualtieri R, Talevi R, Tosti E. Calcium and other ion dynamics during gamete maturation and fertilization. *Theriogenology* 2007; 68:S156–164.
57. Godet M, Sabido O, Gilleron J, Durand P. Meiotic progression of rat spermatocytes requires mitogen-activated protein kinases of Sertoli cells and close contacts between the germ cells and the Sertoli cells. *Dev Biol* 2008; 315:173–188.
58. Sá R, Neves R, Fernandes S, Alves C, Carvalho F, Silva J, Cremades N, Malheiro I, Barros A, Sousa M. Cytological and expression studies and quantitative analysis of the temporal and stage-specific effects of follicle-stimulating hormone and testosterone during cocultures of the normal human seminiferous epithelium. *Biol Reprod* 2008; 79:962–975.
59. La Salle S, Sun F, Handel MA. Isolation and short-term culture of mouse spermatocytes for analysis of meiosis. *Methods Mol Biol* 2009; 558:279–297.
60. Sato T, Katagiri K, Gohbara A, Inoue K, Ogonuki N, Ogura A, Kubota Y, Ogawa T. In vitro production of functional sperm in cultured neonatal mouse testes. *Nature* 2011; 471:504–508.
61. Ventelä S, Toppari J, Parvinen M. Intercellular organelle traffic through cytoplasmic bridges in early spermatids of the rat: mechanisms of haploid gene product sharing. *Mol Biol Cell* 2003; 14:2768–2780.
62. Moens PB, Hugenholtz AD. The arrangement of germ cells in the rat seminiferous tubule: an electron-microscope study. *J Cell Sci* 1975; 19:487–507.
63. Corkidi G, Taboada B, Wood CD, Guerrero A, Darszon A. Tracking sperm in three-dimensions. *Biochem Biophys Res Commun* 2008; 373:125–129.
64. Kopera IA, Bilinska B, Cheng CY, Mruk DD. Sertoli-germ cell junctions in the testis: a review of recent data. *Philos Trans R Soc Lond B Biol Sci* 2010; 365:1593–1605.
65. Wilson JD, Foster DW. *Williams Textbook of Endocrinology*, 8th ed. Philadelphia: W.B. Saunders Company; 1992: 802.